

Sm-doping effect on optical and electrical properties of ZnO films

H. Y. He · J. Fei · J. Lu

Received: 26 November 2014 / Accepted: 7 January 2015 / Published online: 21 January 2015
© The Author(s) 2015. This article is published with open access at Springerlink.com

Abstract A series of ZnO: Sm films with Sm content of 0–1.0 at.% were deposited by a chemical solution deposition. The deposited films were characterized by X-ray diffraction, field emission scanning electron microscopy, UV–Vis and luminescent spectrophotometry, and electrical resistance measurement. The experiments revealed that the Sm doping first increased and then decreased the optical transmittance, band gap, and n-type conductivity with increasing Sm content. The film with the Sm content of 0.75 at.% showed optimal optical and electrical properties. The maximal band gap widening was about 0.19 eV. The resistance decrease of ~ 20 times was observed. The photoluminescence measurement indicated that the films showed a strong near band gap emission and a blue-green emission related to intrinsic defect. The refractive index, extinction coefficient, and dielectric constant of the films were calculated with the transmittance and reflectance spectra.

Keywords ZnO · Sm-doping · Transmittance · Band gap · Luminescence · Electrical resistance

Introduction

Zinc oxide (ZnO) is a wide band gap II–VI semiconductor (3.2–3.37 eV). This material has very attractive properties, including high transparency in the visible wavelength, a high piezoelectric constant, a large electro-optic coefficient [1] and a large exciton binding energy (~ 60 meV) at room temperature. Many studies have recently focused on ZnO

materials because of their potential application in solar cells, gas sensors, piezoelectric transducers and varistors [2–5]. Early studies verified that some dopants, such as Al, In and Ga, can improve the electrical and optical properties of ZnO films [6–8]. Recently, widening in the band gap of ZnO produced by Ti-, Ca-, Si, Sc, and Mo-dopants has also been reported [9–14]. Rare earth cations, such as Tb [15] and Er [16], are more effective. In this work, we focus on the effects of Sm doping on the optical and electrical properties of the ZnO films.

Materials and methods

The starting materials used are all analytic reagents without any further treatment. 0.02 mol ZnNO₃ · 6H₂O was first dissolved in solution of 40 ml ethanol and 40 ml glycol propylene in glass beaker. Subsequently, the Sm₂O₃ for all five samples with Sm content of 0, 0.25, 0.5, 0.75, and 1.0 at.% were dissolved into 10 ml HCl in another glass beaker with constant stirring. The Sm cation solution was expanded to 50 ml with ethanol and added into the four Zn cation solutions at the designed Sm contents by volume. The mixed solutions were then all expanded to 100 ml with ethanol. After a constant stirring of 10 min and an aging of 5 h at room temperature, the solutions were deposited on ultrasonically cleaned glass substrate by dip-coating method. After each coating, the films were dried at 150 °C for 2–5 min. By repeating such dip-coating and drying processes for six times, the films were finally obtained by calcining the dried films at 450 °C for 1.5 h.

The phase and structure of the deposited films were identified at room temperature using an X-ray diffractometer (XRD, CuK_{α1}, $\lambda = 0.15406$ nm, Model No: D/Max-2200PC, Rigaku, Japan). The morphology of the films were

H. Y. He (✉) · J. Fei · J. Lu
College of Materials Science and Engineering, Shaanxi
University of Science and Technology, Xi'an 710021, China
e-mail: hehy@sust.edu.cn

analyzed using a field emission scanning electron microscope (EF-SEM, Model No: JXM-6700F, Japan). The film thickness was determined by a film thickness measuring instrument (Model No: CHY-CB, Labthink, Jinan, China). The light transmittance and reflectance spectra of the films were conventionally recorded on UV–vis spectrophotometer (Model No: UV2600, SDPTOP, Shanghai, Chian). The photoluminescence spectra of the films were measured by a luminescent spectrophotometer (Model no: F-4600, Hitachi, Japan). The electrical resistance of the films was measured by a 4-point probe resistance system (Model No: RTS-9, Probes Tech, Guangzhou, China).

Results and discussion

Microstructural characterization of the films

Figure 1 shows the XRD patterns of the films. The wurtzite ZnO is the only XRD detectable phase of the films (JCPDS card No: 36-1451). Obvious *c*-orientation decreased as increasing Sm content is observed for the films with the Sm contents of 0, 0.25, and 0.50 at.%. This *c*-orientation transforms to a weak *a*-orientation as the Sm content is over 0.75 at.%. The formation of the *c*-orientation could be associated to the rapid heating rate in the calcination process and the lattice parameter matching between the films and substrate [17]. Whereas the transformation to *a*-orientation could be related to the slowdown of the ZnO crystallization (the decrease of the crystallinity) and the variation of lattice parameter resulted from Sm-doping. Crystallites size (*D*) was obtained according to the Scherrer's equation

$$D = 0.9 \frac{\lambda}{\beta \cos \theta} \quad (1)$$

where λ is the X-ray wavelength, β the full width at half maximum of the considered peak and θ is the Bragg angle. Since wurtzite ZnO is a hexagonal crystal, the lattice parameters of the films can be calculated with XRD data analysis by following equation:

$$\frac{a^2}{d^2} = \frac{4}{3} (h^2 + hk + k^2) + \frac{a^2}{c^2} l^2 \quad (2)$$

The calculated lattice parameters and average particle sizes of the films are listed in Table 1. The average particle size overall decreases as increasing Sm content, which could be ascribed to the interference of the Sm cation to the ZnO crystal growth. This interference effect could be associated with the crystal lattice distortion due to the larger ionic radius of Sm^{3+} (1.04 Å) compared with Zn^{2+} (0.74 Å). The lattice expands as the increase of Sm content, which is also due to larger ion radius of Sm^{3+} cation than that of Zn^{2+} cation and the decrease of the crystallinity.

Figure 2 shows the SEM micrographs of the films. The films are composed of small hexagonal and granular morphology particles and some larger hexagonal rodlike particles. The hexagonal granular particles in the films with Sm content of 0–0.50 at.% could also have rodlike morphology and is approximately perpendicular to the substrate and the rodlike morphology and its disappearance with Sm doping could correspond to the *c*-orientation and *a*-orientation, respectively. Average particle size decreases with increasing Sm content. This is consistent with the results calculated with the XRD data analysis. The grains appear larger than average particle size than the results estimated with the XRD data analysis, which could imply that the nanoparticles in the films are polycrystalline. The measured film thicknesses are in a range of ~835–920 nm as listed in Table 1.

Optical property of the films

Figure 3a, b shows the transmittance (*T*) and reflectance (*R*) spectra of the ZnO: Sm films. Their average values in the wavelength range of 280–840 nm are listed in Table 2. The average transmittances are in the range of ~59.4–74.2 %. They first increase and then decrease with increasing Sm content and show the maximum as Sm content equals 0.75 at.% (Fig. 3a). The increase of transmittance with respect to the pure ZnO film may be related to the well-known Moss–Burstein effect and the decrease of crystallinity. Moreover, the light adsorption

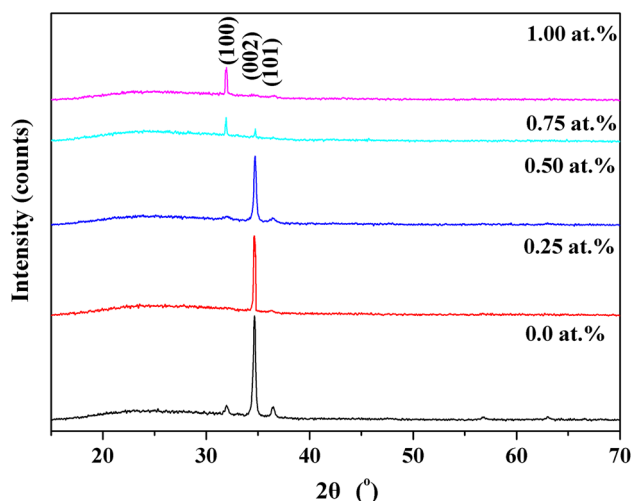


Fig. 1 XRD patterns of the films deposited from solution with various Sm contents



Table 1 Lattice parameter, average particle size and thickness of the ZnO films deposited from solutions with various designed Sm contents (at.%)

Sm content	Lattice parameter (Å)		Particle size (nm)				Thickness (nm)
	<i>a</i>	<i>c</i>	(100)	(002)	(101)	Average	
0	3.2309	5.1718	22.0	31.6	23.9	25.8	920
0.25	3.2342	5.1741	–	36.0	16.2	26.1	895
0.50	3.2365	5.1766	14.4	30.1	14.3	19.6	885
0.75	3.2382	5.1802	22.1	19.8	21.1	21.0	865
1.00	3.2327	5.1830	24.9	18.0	16.4	19.8	835

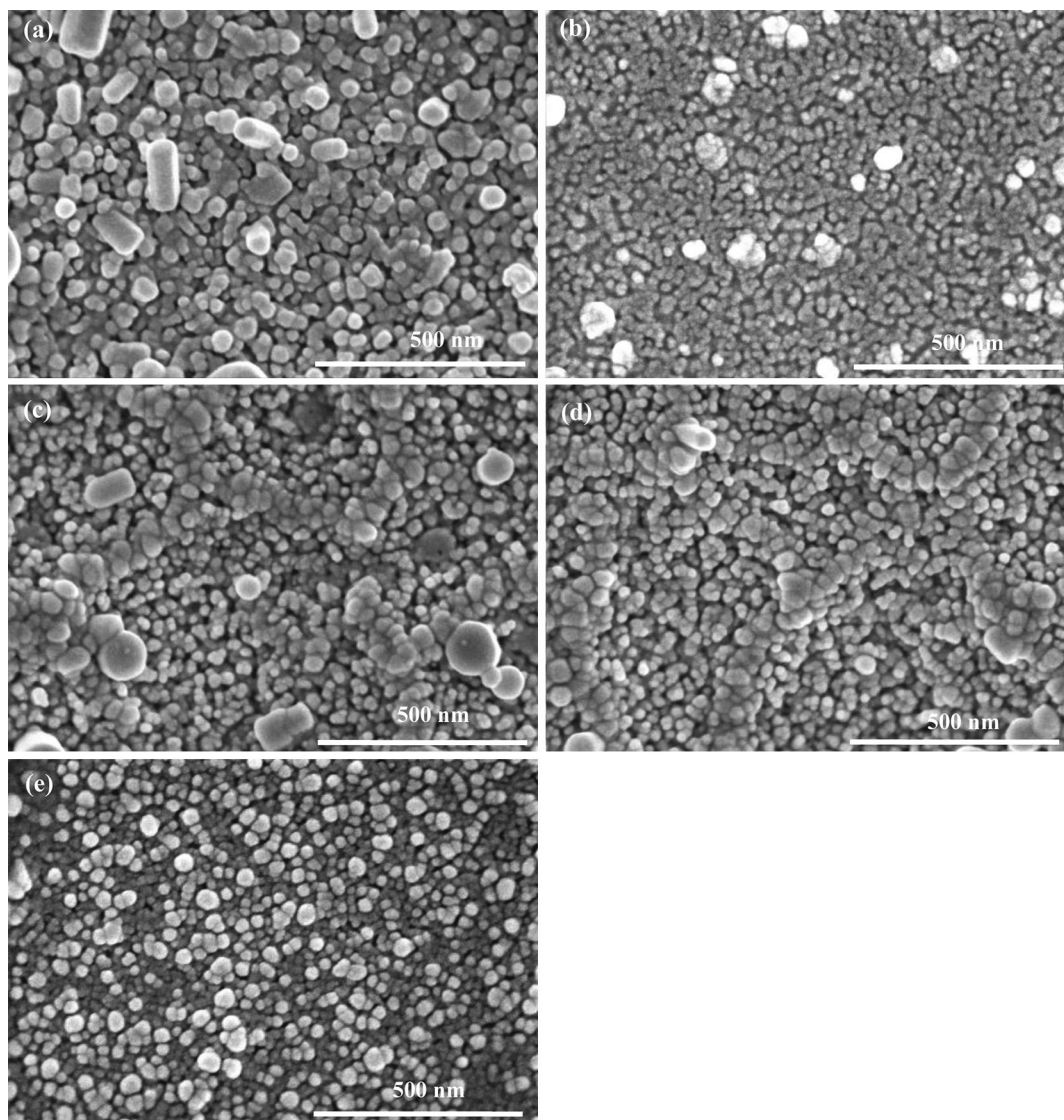


Fig. 2 SEM micrographs of the films deposited from solution with Sm contents of **a** 0 at.%, **b** 0.25 at.%, **c** 0.5 at.%, **d** 0.75 at.% and **e** 1.0 at.%

edge first blue-shifts and then red-shifts with the increase of Sm content. Wurtzite ZnO has a direct band gap, so that the optical band gap (E_g) can be calculated with Tauc's relationship [18]:

$$(\alpha hv)^2 = C(hv - E_g) \quad (4)$$

where hv is photon energy, C is a constant, and α is absorption coefficient. The α can be calculated by equation [19]:

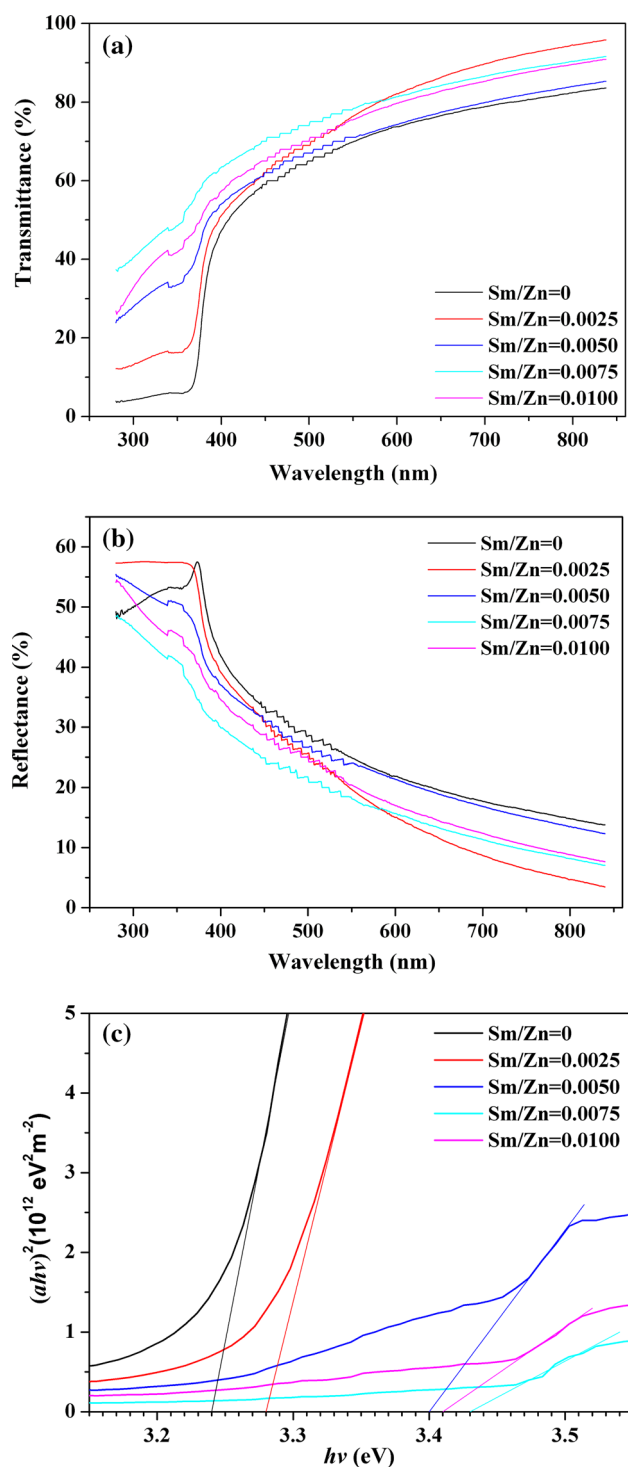


Fig. 3 **a** Transmittance (T), **b** absorbance (A), **c** graphs of $(\alpha hv)^2$ vs. photon energy hv

$$\alpha = \frac{1}{d} \ln \frac{1-R}{T} \quad (5)$$

where d is the film thickness. Figure 3c shows the graphs of $(\alpha hv)^2$ versus photon energy hv . The linear dependences of $(\alpha hv)^2$ on hv at higher photon energies

indicate that the films are essentially direct-transition-type semiconductors. The straight-line portion of the curve, when extrapolated to zero, gives the optical band gap E_g . The estimated E_g are in the range of ~ 3.24 – 3.43 eV (Table 2). Maximal widening (0.19 eV) is achieved as Sm content equals 0.75 at.%. This widening is larger than the reported 0.018 eV and 0.04 eV resulted from Al doping of 2–3 at.% [20, 21] and near 0.21 eV due to Er dopings of 0.6 at.% [19]. The band gap widening with respect to the pure ZnO film may be the well-known Moss–Burstein shift [13–16, 19]. In addition, the band gap is also associated with the particle size and lattice parameter. The decrease of the average particle size as the increase of Sm content can widen the band gap due to quantum refinement effect. Whereas the lattice expansion as the increase of Sm content can narrow the band gap due to decreased interaction between atoms.

Optical constants, refractive index (n) and extinction coefficient (k), of the pure and doped ZnO films can be calculated on basis of relations [19, 22],

$$n = \frac{1 + R^{1/2}}{1 - R^{1/2}} \quad (6)$$

$$k = \frac{\alpha \lambda}{4\pi} \quad (7)$$

Their variations with incident photon hv are shown in Fig. 4. The n and k values first decrease and then increase as increasing Sm content, which is consistent with the variations of the R and A . In addition, the n and k values are also related with the lattice parameter [22]. The dielectric constant (ϵ) of the films are determined with the relation [19, 22].

$$\epsilon = \epsilon_r + i\epsilon_i = (n + ik)^2 \quad (8)$$

where ϵ_r is the real part and is the normal dielectric constant, ϵ_i is the imaginary part and represents the dielectric loss. The variations of the ϵ_r and ϵ_i with incident photon hv are shown in Fig. 5 and are also mainly dependent on the light absorption of the films. In addition, the ϵ_r and ϵ_i should also be associated with the lattice parameter and particle size. In general, larger lattice parameter (low crystallinity) results in smaller light absorption and so smaller ϵ_r and ϵ_i , while single-domain size leads to largest coercive field and so largest ϵ_r and ϵ_i , and smaller particle size leads to larger domain wall concentration and so larger ϵ_r and ϵ_i .

Figure 6 illustrates the photoluminescence spectra of the ZnO: Sm films. The strong emission peaks centered at ~ 386 and ~ 494 nm are observed. The emission intensities overall first obviously increase as increasing Sm content to 0.5 at.% and then decrease as further increasing Sm content. In general, smaller particle size corresponds a



Table 2 The average values of optical parameters in the range of 280–840 nm, band gap energy (E_g) of the ZnO: Sm films

Sm content (at.%)	T (%)	R (%)	E_g (eV)	n	$k \times 10^{-3}$	ε_r	$\varepsilon_i \times 10^{-2}$
0	59.4	29.0	3.24	3.6	12.4	14.8	13.8
0.25	67.9	24.4	3.28	3.2	6.3	14.9	7.6
0.50	65.8	27.4	3.40	3.4	4.3	13.4	3.7
0.75	74.2	21.1	3.43	2.8	2.5	9.0	1.8
1.00	70.8	23.6	3.41	3.1	3.2	11.0	2.6

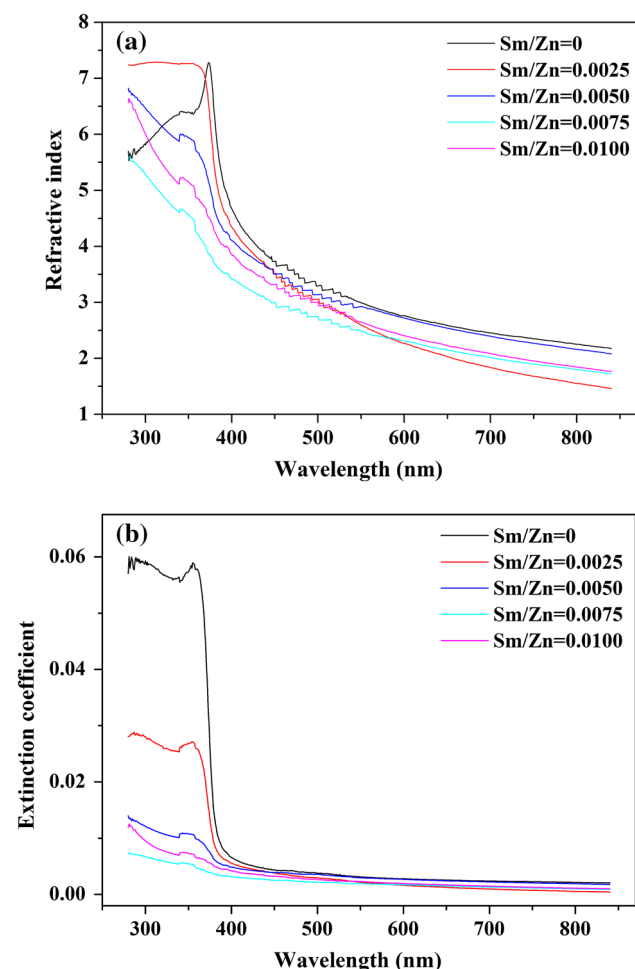


Fig. 4 a Refractive index and b extinction coefficient of the films with various Sm contents

larger specific surface area and thereby leading to larger emission intensity, however too small particle size leads to large light scattering that decreasing emission intensity. Thus, the variation of the emission intensity with Sm content could be ascribed to the variation of the average particle size with Sm content. The emissions centered at ~ 386 nm (~ 3.21 eV) could be near band gap emission [23] or band edge emission [24]. The emissions centered at ~ 494 nm (~ 2.51 eV) could be related to the energy interval from the Zn interstitial to the Zn vacancy level (~ 2.6 eV [25, 26]).

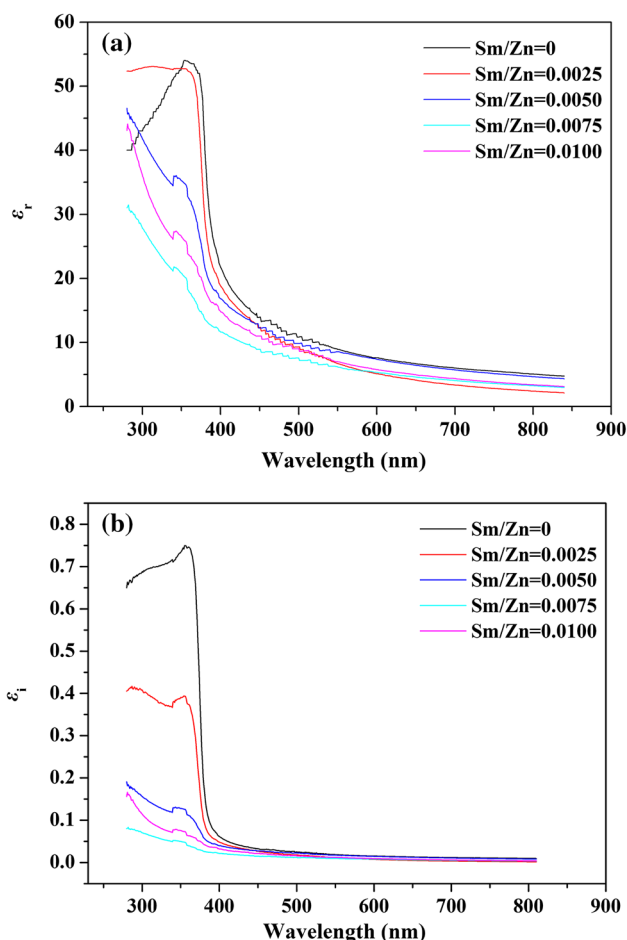


Fig. 5 a Real part and b imaginary part of dielectric constant of the ZnO: Sm films vs. incident photon $h\nu$

Electrical property

The variation of electrical resistivity with Sm content is shown in Fig. 7. The resistivity of the films first obviously decreases from $\sim 5.61 \times 10^{-2} \Omega \text{ cm}$ to $\sim 0.28 \times 10^{-2} \Omega \text{ cm}$ and increases to $\sim 0.88 \times 10^{-2} \Omega \text{ cm}$ with the increase of Sm content. The film with Sm-content of 0.75 at.% shows a minimal resistivity. The increase in electrical conductivity could originate from the increase of the large carrier concentration introduced by trivalent Sm^{3+} cation. This also might imply that the films are n-type conductive. The resistivity of the ZnO films is associated with preparation method



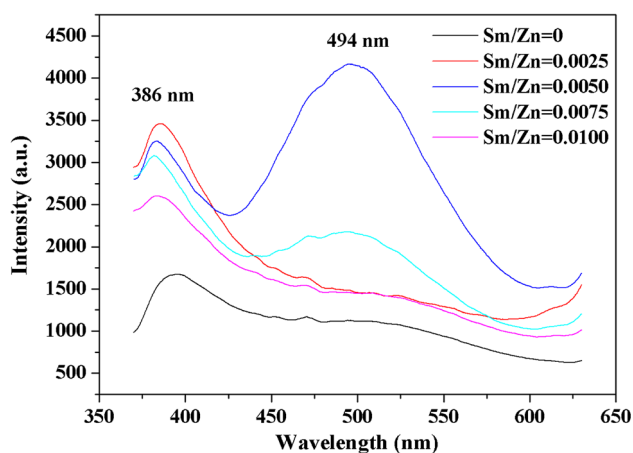


Fig. 6 Photoluminescence spectra of the ZnO: Sm films

and processing parameter. A resistivity of 6.44×10^{-2} to $4.44 \times 10^{-5} \Omega \text{ cm}$ is reported for RF magnetron sputtered ZnO: Co films [27]. Another RF magnetron sputtered ZnO: Ga film showed a resistivity of $\sim 5.3 \times 10^{-2}$ to $8.4 \times 10^{-4} \Omega \text{ cm}$ [28]. A ZnO film deposited by ultra-high frequency spraying process at 480°C doped with 1.9 % copper and annealed for 10 h at 700°C exhibits a resistivity as high as $5.6 \times 10^{12} \Omega \text{ cm}$ [29].

The deterioration of the optical transmittance and electrical conductivity of the films with excessively increasing Sm content could be ascribed to the electron-impurity interaction and the coulombic interaction between the carriers [24].

Conclusions

The effects of Sm doping on the microstructure and optical and electrical properties of the ZnO films were investigated. With increasing Sm content, the average particle size decreased, and the transmittance in the range of UV–visible light and band gap was first increased and then decreased. The Sm content of 0.75 at % led to maximal transmittance and widened band gap of from 3.24 eV of the pure film to 3.43 eV. Moreover, the resistivity of the films was in the range of $0.28\text{--}6.51 \times 10^{-2} \Omega \text{ cm}$ and also first decreased and then increased with increasing Sm content. The decrease of resistivity with the increase of carrier concentration resulted from Sm doping indicated that the films are n-type conductive. Furthermore, the films showed strong near band gap emission centered at 386 nm and blue-green emission centered at 494 nm. The refractive index, extinction coefficient, optical conductivity, and dielectric constant of the films were calculated with the transmittance and reflectance spectra. Improved optical and electrical properties by Sm doping may be of significance

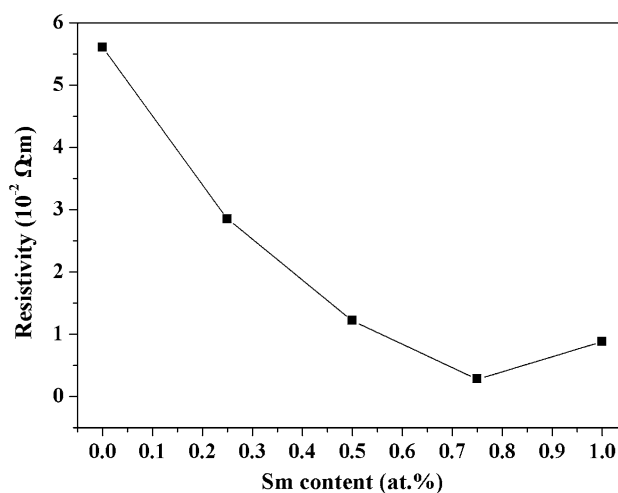


Fig. 7 Electrical resistivity of the films vs. Sm contents

to the optical and electrical applications of the Sm-doped ZnO materials.

Open Access This article is distributed under the terms of the Creative Commons Attribution License which permits any use, distribution, and reproduction in any medium, provided the original author(s) and the source are credited.

References

- Polla, D.L., Muller, R.S., White, R.M.: Integrated multisensor chip. *IEEE Electron Device Lett.* **7**, 254–256 (1996). doi:10.1109/EDL.1986.26363
- BeekE, W.J., Wienk, M.M., Janssen, R.A.J.: Hybrid solar cells from regioregular polythiophene and ZnO nanoparticles. *Adv. Funct. Mater.* **16**, 1112–1116 (2006). doi:10.1002/adfm.200500573
- Wang, Z.-L., Song, J.-H.: Piezoelectric nanogenerators based on zinc oxide nanowire arrays. *Science* **312**, 242–246 (2006). doi:10.1126/science.1124005
- Wang, J.-X., Sun, X.-W., Yang, Y., Huang, H., Lee, Y.C., Tan, O.-K., Vayssieres, L.: Hydrothermally grown oriented ZnO nanorod arrays for gas sensing applications. *Nanotech* **17**, 4995–4998 (2006). doi:10.1088/0957-4484/17/19/037
- Liu, H.-Y., Kong, H., Ma, X.-M., Shi, W.-Z.: Microstructure and electrical properties of ZnO-based varistors prepared by high-energy ball milling. *J. Mater. Sci.* **42**, 2637–2642 (2007). doi:10.1007/s10853-006-1350-7
- Terasako, T., Song, H., Makino, H., Shirakata, S., Yamamoto, T.: Temperature dependence of electrical properties of Ga-doped ZnO films deposited by ion plating with DC arc discharge. *Thin Solid Films* **528**, 19–25 (2013). doi:10.1016/j.tsf.2012.07.140
- Nunes, P., Fernandes, B., Fortunan, E., Vilarinlo, P., Martins, R.: Performances presented by zinc oxide thin films deposited by spray pyrolysis. *Thin Solid Films* **337**, 176–179 (1999). doi:10.1016/S0040-6090(98)01394-7
- Reddy, K.T.R., Miles, R.W.: Growth and characterization of sprayed ZnO: Ga thin films. *J. Mater. Sci. Lett.* **17**, 279–281 (1998). doi:10.1023/A:1006569203107
- Lin, S.-S., Huang, J.-L., Sajgalik, P.: The properties of Ti-substituted ZnO films deposited by simultaneous RF and DC

- magnetron sputtering. *Surf. Coat. Tech.* **191**, 286–292 (2005). doi:[10.1016/j.surfcoat.2004.03.021](https://doi.org/10.1016/j.surfcoat.2004.03.021)
10. Misra, K.P., Shukla, R.K., Srivastava, A., Srivastava, A.: Blue-shift in optical band gap in nanocrystalline $Zn_{1-x}Ca_xO$ films deposited by sol-gel method. *Appl. Phys. Lett.* **95**(3), 031901–031905 (2009). doi:[10.1063/1.3184789](https://doi.org/10.1063/1.3184789)
 11. Das, A.K.: Misra P and Kukreja L.M.: Effect of Si doping on electrical and optical properties of ZnO thin films grown by sequential pulsed laser deposition. *J. Phys. D Appl. Phys.* **42**, 165405–165411 (2009). doi:[10.1088/0022-3727/42/16/165405](https://doi.org/10.1088/0022-3727/42/16/165405)
 12. Minami, T., Yamamoto, T., Miyata, T.: Highly transparent and conductive rare earth-doped ZnO thin films prepared by magnetron sputtering. *Thin Solid Films* **366**, 63–68 (2000). doi:[10.1016/S0040-6090\(00\)00731-8](https://doi.org/10.1016/S0040-6090(00)00731-8)
 13. Wu, C.-G., Shen, J., Ma, J., Wang, S.-P., Zhang, Z.-J., Yang, X.-L.: Electrical and optical properties of molybdenum-doped ZnO transparent conductive thin films prepared by dc reactive magnetron sputtering. *Semicond. Sci. Technol.* **24**, 125012–125017 (2009). doi:[10.1088/0268-1242/24/12/125012](https://doi.org/10.1088/0268-1242/24/12/125012)
 14. Lin, Y.-C., Wang, B.-L., Yen, W.-T., Ha, C.-T., Peng, C.: Effect of process conditions on the optoelectronic characteristics of ZnO:Mo thin films prepared by pulsed direct current magnetron sputtering. *Thin Solid Films* **518**, 4928–4934 (2010). doi:[10.1016/j.tsf.2010.03.007](https://doi.org/10.1016/j.tsf.2010.03.007)
 15. Fang, Z.-B., Tan, Y.-S., Gong, H.-X., Zhen, C.-M., He, Z.-W., Wang, Y.-Y.: Transparent conductive Tb-doped ZnO films prepared by rf reactive magnetron sputtering. *Mater. Letters* **59**, 2611–2614 (2005). doi:[10.1016/j.matlet.2005.02.062](https://doi.org/10.1016/j.matlet.2005.02.062)
 16. Kumari, V., Kumar, V., Malik, B.P., Mehra, R.M., Mohan, D.: Nonlinear optical properties of erbium doped zinc oxide (EZO) thin films. *Opt. Commun.* **285**, 2182–2188 (2012). doi:[10.1016/j.optcom.2011.12.094](https://doi.org/10.1016/j.optcom.2011.12.094)
 17. He, H.Y., Yu, H.Y.: Enhancement in optical transmission of ZnO:Al film by c-orientation arrayed growth. *Int. J. Mat. Res.* **102**(5), 556–559 (2011). doi:[10.3139/146.110414](https://doi.org/10.3139/146.110414)
 18. Chen, J.L., Chen, D., He, J.J., Zhang, S.Y., Chen, Z.H.: The microstructure, optical, and electrical properties of sol-gel-derived Sc-doped and Al-Sc co-doped ZnO thin films. *Appl. Surf. Sci.* **255**, 9413–9419 (2009). doi:[10.1016/j.apsusc.2009.07.044](https://doi.org/10.1016/j.apsusc.2009.07.044)
 19. Pathan, H.M., Desai, J.D., Lokhande, C.D.: Modified chemical deposition and physico-chemical properties of copper sulphide (Cu_2S) thin films. *Appl. Surf. Sci.* **202**, 47 (2002). doi:[10.1016/S0169-4332\(02\)00843-7](https://doi.org/10.1016/S0169-4332(02)00843-7)
 20. Korake, P.V., Dhabbe, R.S., Kadam, A.N., Gaikwad, Y.B., Garadkar, K.M.: Highly active lanthanum doped ZnO nanorods for photodegradation of metasytox. *J. Photochem. Photobiol., B* **130**, 11–19 (2014). doi:[10.1016/j.jphotobiol.2013.10.012](https://doi.org/10.1016/j.jphotobiol.2013.10.012)
 21. Chaki, S.H., Deshpande, M.P., Tailor, J.P.: Characterization of CuS nanocrystalline thin films synthesized by chemical bath deposition and dip coating techniques. *Thin Solid Films* **550**, 291–297 (2014). doi:[10.1016/j.tsf.2013.11.037](https://doi.org/10.1016/j.tsf.2013.11.037)
 22. Luo, Z.-D., Huang, Y.-D.: Qualitative analysis of relationship between refractive index and atomic parameters of solid materials. *J. Rare Earths* **22**, 486–488 (2004)
 23. Wraback, M., Shen, H., Liang, S., Gorla, C.R., Lu, Y.: High contrast, ultrafast optically addressed ultraviolet light modulator based upon optical anisotropy in ZnO films grown on R-plane sapphire. *Appl. Phys. Lett.* **74**, 507 (1999). doi:[10.1063/1.124223](https://doi.org/10.1063/1.124223)
 24. Schaadt, D.M., Brandt, O., Ghosh, S., Flissikowski, T., Jahn, U., Grahm, H.T.: Polarization-dependent beam switch based on an M-plane GaN/AlN distributed Bragg reflector. *Appl. Phys. Lett.* **90**, 231117 (2007). doi:[10.1063/1.2747189](https://doi.org/10.1063/1.2747189)
 25. Xu, P.-S., Sun, Y.-M., Shi, C.-S., Xu, F.-Q., Pan, H.-B.: The electron structures of ZnO and its defects. *Sci. Chin. A* **31**(4), 358–365 (2001)
 26. Lin, B.-X., Fu, Z.-X.: Green luminescent center in undoped zinc oxide films deposited on silicon substrates. *Appl. Phys. Lett.* **79**, 943–945 (2001). doi:[10.1063/1.1394173](https://doi.org/10.1063/1.1394173)
 27. Güner, S., Gürbüz, O., Çalışkan, S., Nuzhdin, V.I., Khaibullin, R., Öztürk, M., Akdoğan, N.: The structural and magnetic properties of Co^{+} implanted ZnO films. *Appl. Surf. Sci.* **310**, 235–241 (2014). doi:[10.1016/j.apsusc.2014.03.085](https://doi.org/10.1016/j.apsusc.2014.03.085)
 28. Chang, S.H., Cheng, H.-M., Tien, C.-L., Lin, S.-C., Chuang, K.-P.: Optical, electrical and mechanical properties of Ga-doped ZnO thin films under different sputtering powers. *Opt. Mater.* **38**, 87–91 (2014). doi:[10.1016/j.optmat.2014.10.004](https://doi.org/10.1016/j.optmat.2014.10.004)
 29. Labeau, M., Rey, P., Deschanvres, J.L., Joubert, J.C., Delabouglise, G.: Thin films of high-resistivity zinc oxide produced by a modified CVD method. *Thin Solid Films* **213**, 94 (1992). doi:[10.1016/0040-6090\(92\)90480-Y](https://doi.org/10.1016/0040-6090(92)90480-Y)

